Supplement of Geosci. Model Dev., 14, 7775–7793, 2021
https://doi.org/10.5194/gmd-14-7775-2021-supplement

Geoscientific Model Development
Open Access

Supplement of

How well can inverse analyses of high-resolution satellite data resolve heterogeneous methane fluxes? Observing system simulation experiments with the GEOS-Chem adjoint model (v35)

Xueying Yu et al.

Correspondence to: Dylan B. Millet (dbm@umn.edu)

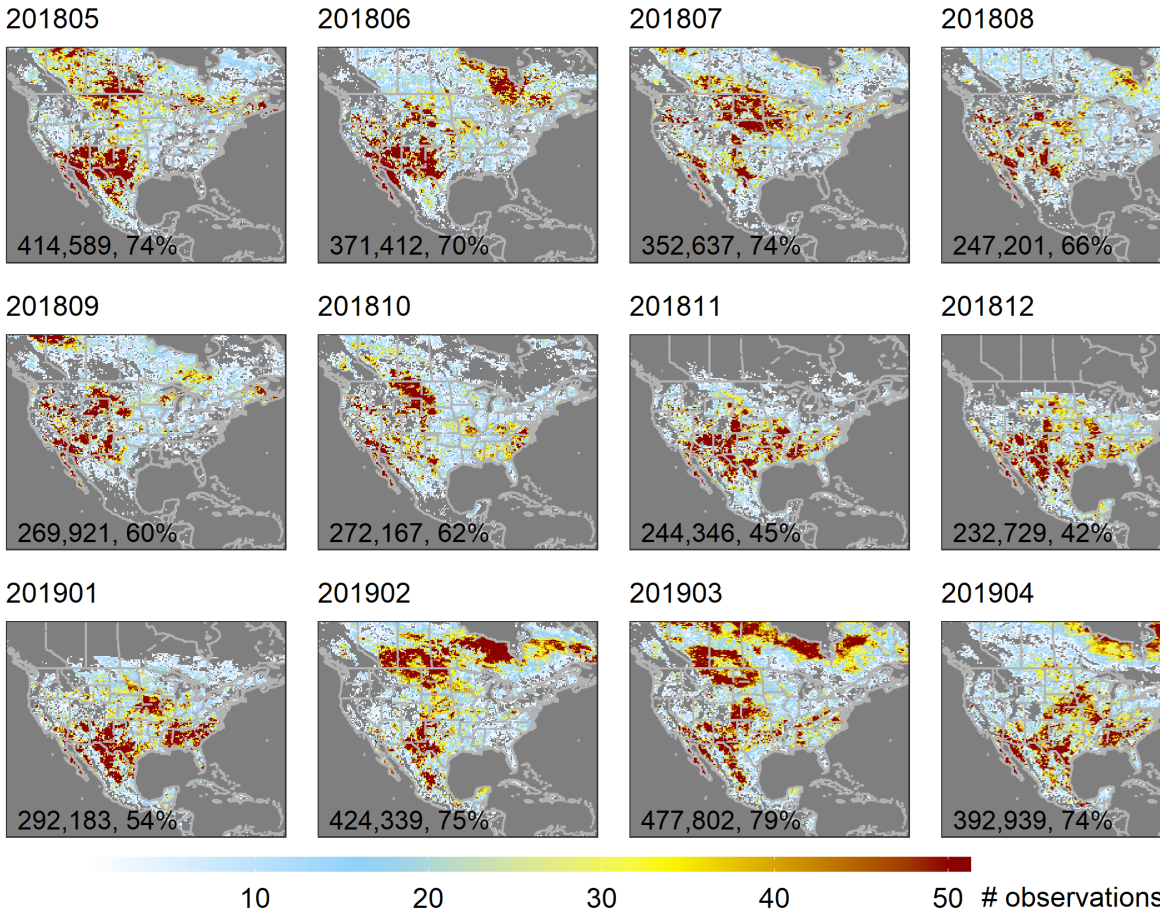

Figure S1. Monthly TROPOMI sampling density at 0.25° × 0.3125° resolution (~25 km) between May 2018 and April 2019, after filtering for data quality and clouds. The total number of observations, and percent over-land grid cell data coverage, is indicated in each panel.

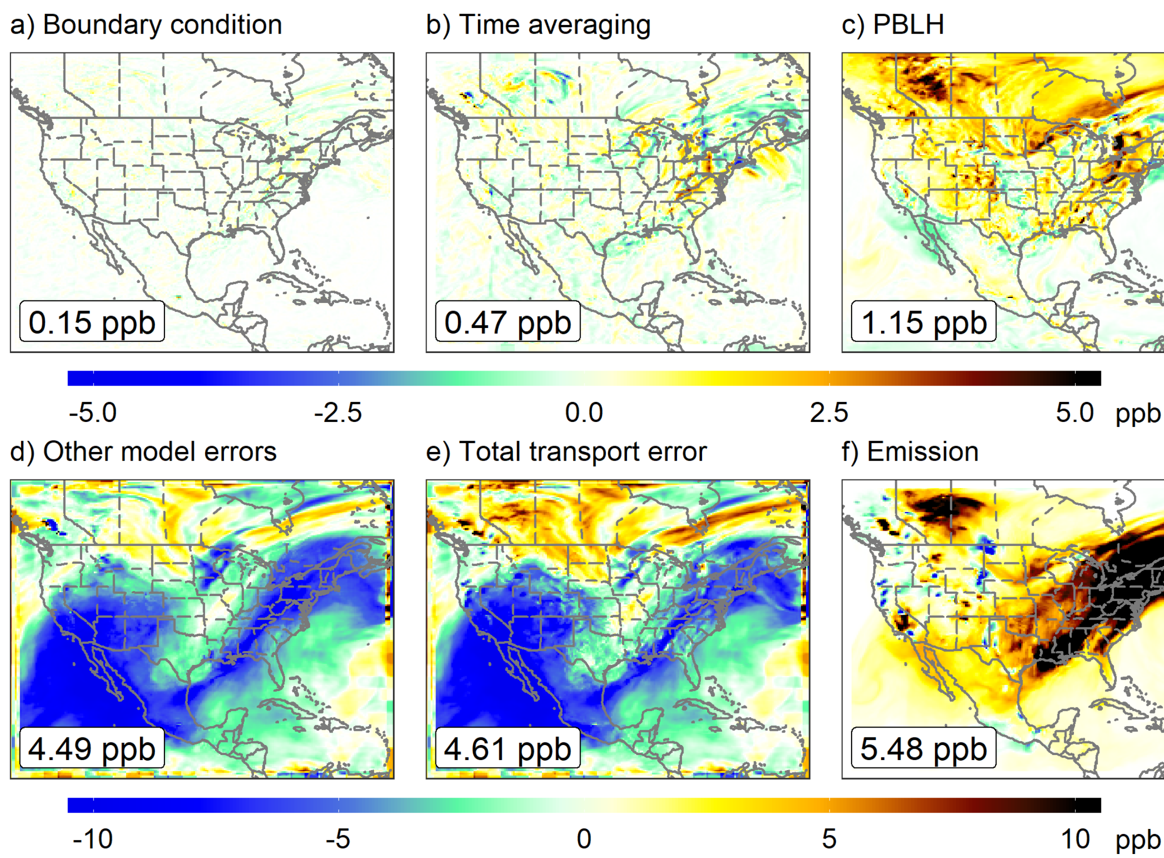

Figure S2. Methane column concentration differences for 2018-08-01 resulting from the individual model transport errors employed in the OSSE (see Sect. 2 for details). Shown are differences incurred from: a) using 6 versus 3 buffer grid cells at the domain boundary; b) averaging over 13:00-14:00 LT versus sampling the model instantaneously at the satellite overpass time; c) employing non-local versus full PBL mixing schemes; d) alternate convection and tropopause treatments; and e) all model transport errors. Shown for comparison are f) the column differences that arise from employing the true versus spatially biased prior emissions. The root-mean-square errors (RMSE) relative to the true fluxes are labeled in each panel.

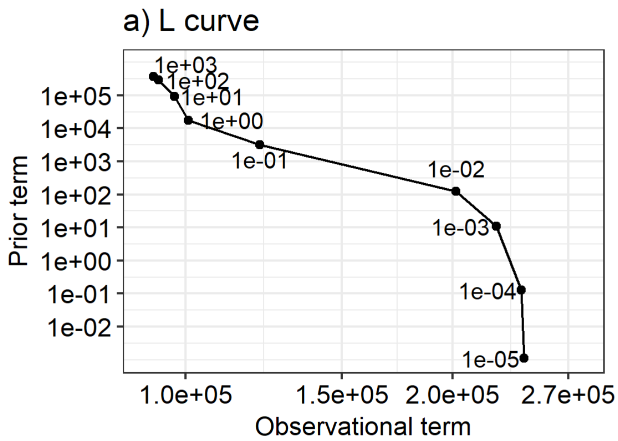

Figure S3. Cost function analysis and determination of the regularization parameter γ based on one-week inversions with spatially uniform prior errors. Panel a) shows the L curve comparing the prior and observational deviation terms in the cost function as a function of γ, following the method in Hansen and O'Leary (1993). As shown in Eq. 1 of the main text, the prior term is given by $(\boldsymbol{x} - \boldsymbol{x_a})^{\mathrm{T}}\mathbf{S_a^{-1}}(\boldsymbol{x} - \boldsymbol{x_a})$ and the observational term is given by $\left(\boldsymbol{y} - F(\boldsymbol{x})\right)^{\mathrm{T}}\mathbf{S_{obs}^{-1}}(\boldsymbol{y} - F(\boldsymbol{x}))$. Panel b) shows the prior term divided by the total cost function computed at γ = 1000 (J_{1000}, where the solution is mostly determined by the observations; blue line), the observational term divided by the total cost function computed at γ = 0 (J_0, where the solution is solely determined by the prior; red line), and the sum of the blue and red lines (in grey).

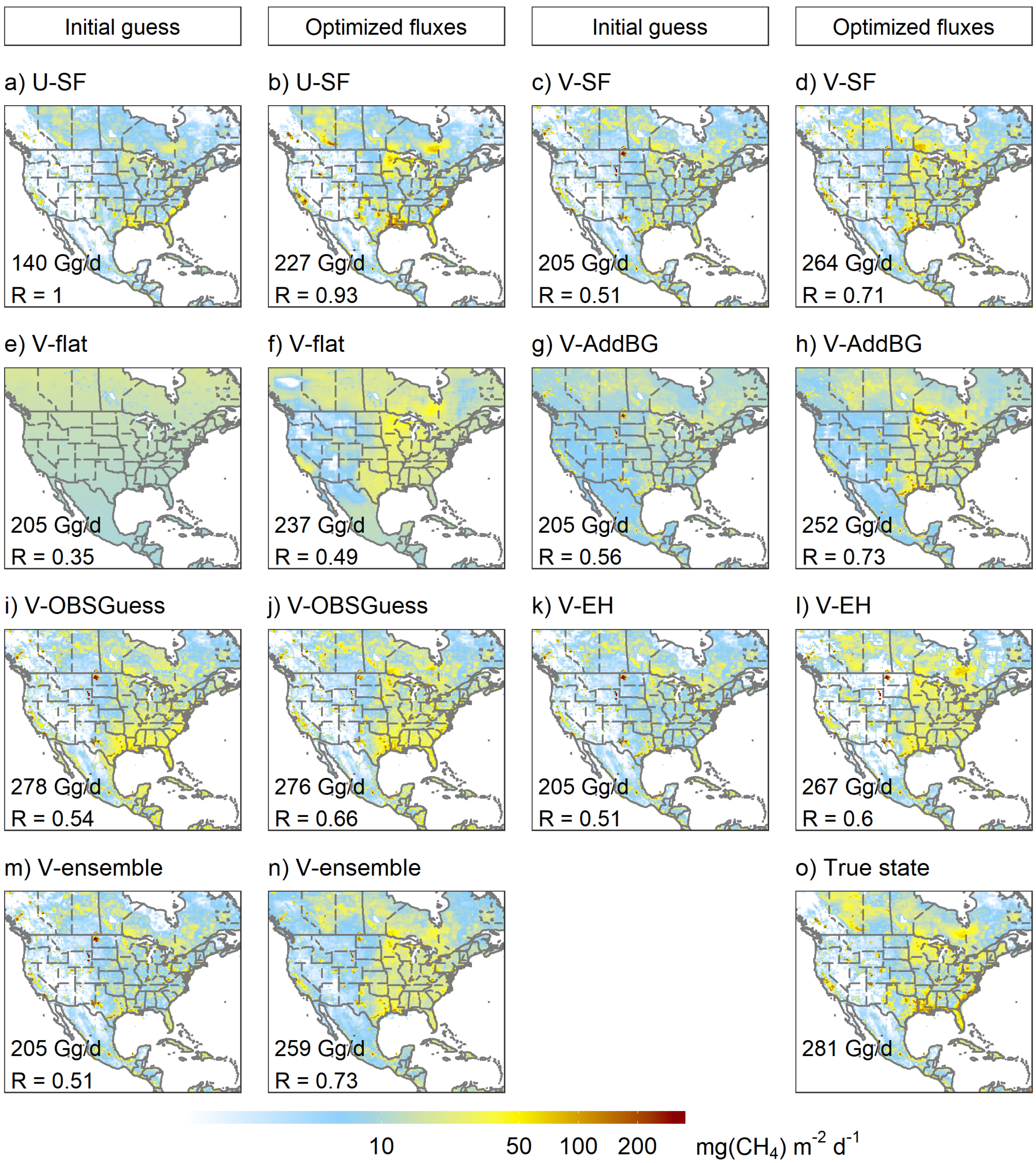

Figure S4. Initial guess and optimized emissions for each inversion framework. Labels inset indicate the domain-wide total emissions and spatial correlation to the true fluxes.

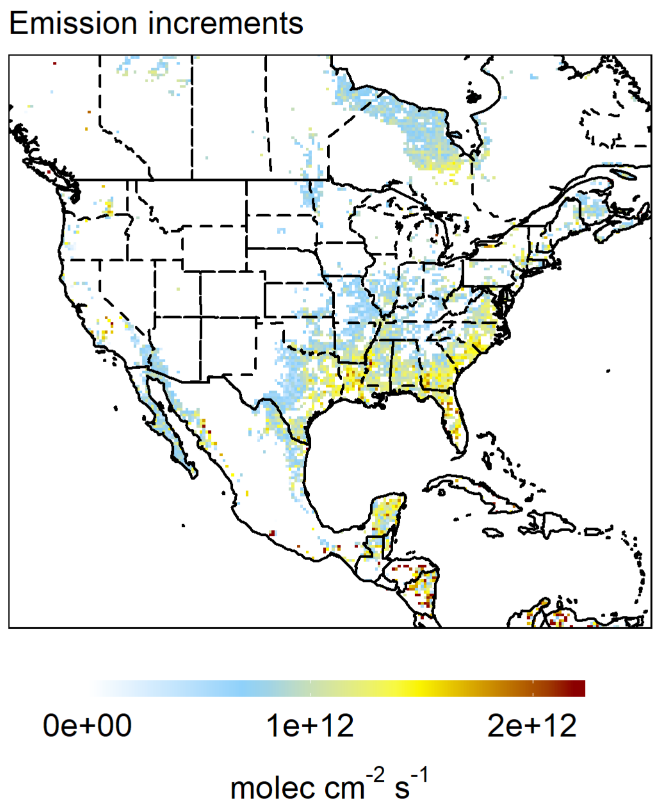

Figure S5. Emission increments added to the prior fluxes in the V-OBSGuess inversions. See Sect. 4 for details.

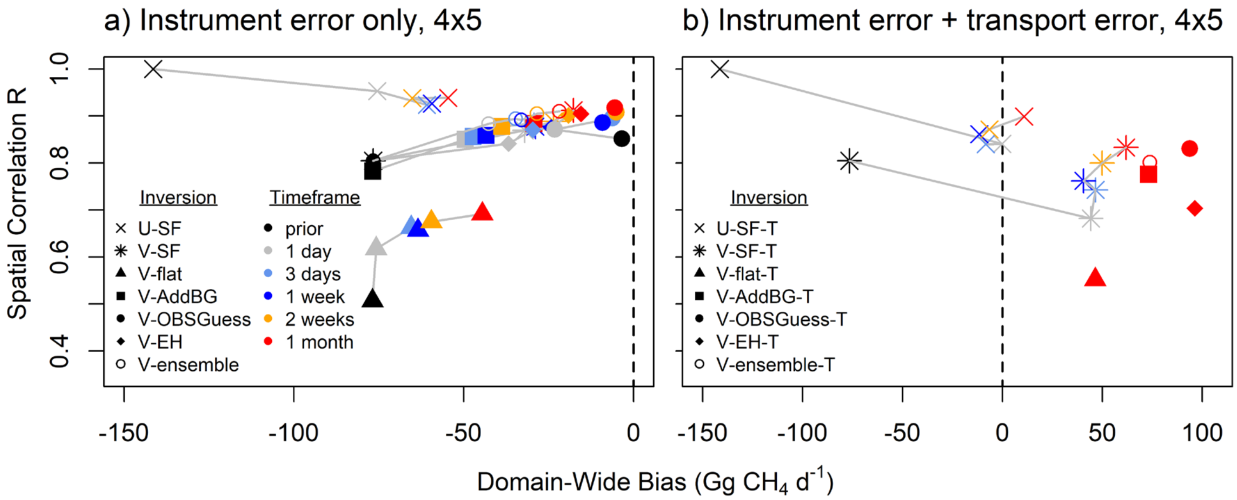

Figure S6. Same as Figure 8, but with prior and posterior results degraded to 4°×5° horizontal resolution.

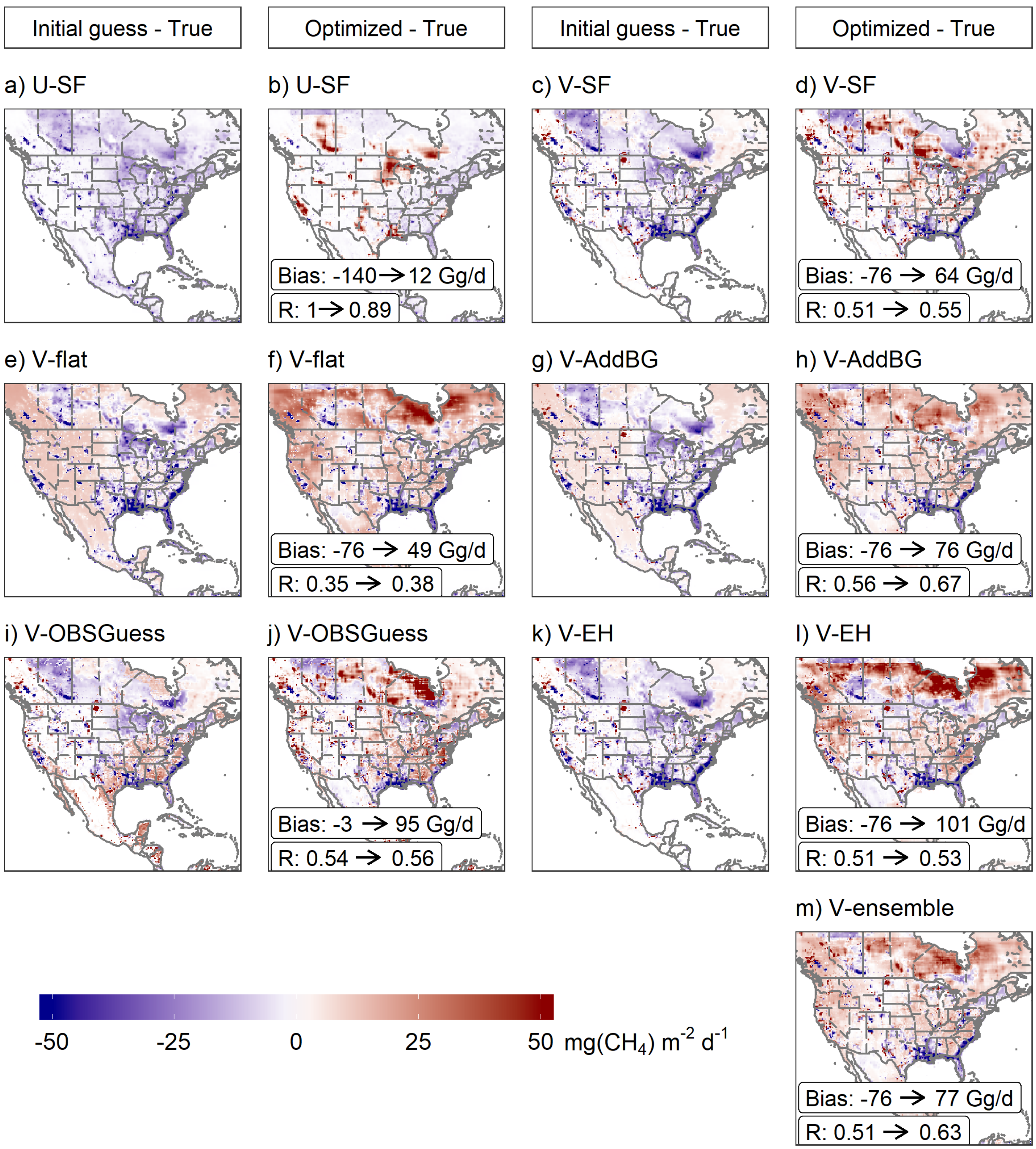

Figure S7. Same as Fig. 4, but showing results with model transport error.

Table S1. Filters applied for TROPOMI data quality assurance

Parameter	Range
Solar Zenith Angle (SZA)	≤ 70°
Viewing Zenith Angle (VZA)	≤ 60°
Surface albedo	≥ 0.02
Aerosol Optical Thickness (AOT)	< 0.3
XCH_4 precision (noise-related error)	< 10 ppb
Signal-to-noise ratio	≥ 50
χ^2	< 100
Fraction of non-corrupted/unphysical spectral pixel[1]	≥ 70%
Cloudiness level	Confidently clear[1]

[1]Pixel quality is determined per orbit, for details see the TROPOMI Product User Manual (2019).

Reference

Hansen, P. C., and O'Leary, D. P.: The Use of the L-Curve in the Regularization of Discrete Ill-Posed Problems, SIAM Journal on Scientific Computing, 14(6), 1487-1503, 10.1137/0914086, 1993.

TROPOMI product user manual: http://www.tropomi.eu/data-products/methane/, last access: 15 April 2019.